Evaluation of relaxation dynamics from excited states of Ho^{3+} ions in sol-gel nano-glass-ceramic materials

Natalia Pawlik[1,*], Joanna Śmiarowska[1], Bartosz Handke[2], Maciej Zubko[3,4], Maciej Sitarz[2], Wojciech A. Pisarski[1]

[1] University of Silesia, Institute of Chemistry, 9 Szkolna Str., 40-007 Katowice, Poland
[2] AGH University of Krakow, Faculty of Materials Science and Ceramics, 30 Mickiewicza Av., 30-059 Kraków, Poland
[3] University of Silesia, Institute of Materials Engineering, 75. Pułku Piechoty 1A Str., 41-500 Chorzów, Poland
[4] University of Hradec Králové, Department of Physics, Rokitanského 62, 50003 Hradec Králové, Czech Republic

SUPPLEMENTAL INFORMATION

1. Supporting information on structural analysis

Table S1. Parameters determined for LaF_3 nanocrystals with trigonal symmetry (crystallized in $P\bar{3}c1$ space group) fabricated Ho^{3+}-doped sol-gel materials.

Series	Sample	Average crystallite size [nm]	Lattice parameters			Unit cell volume [Å^3]	R [%]
			α, β, γ	$a = b$ [Å]	c [Å]		
SiO_2-LaF_3:Ho^{3+} (700°C)	$GC1_{700}$	6.48	$\alpha = \beta = 90°$ $\gamma = 120°$	7.186(4)	7.345(5)	328.44	9.56
	$GC2_{700}$	-		-	-	-	-
	$GC3_{700}$	9.96		7.192(2)	7.353(3)	329.36	9.64
	$GC4_{700}$	8.11		7.187(4)	7.350(5)	328.77	10.21
	$GC5_{700}$	-		-	-	-	-
	$GC6_{700}$	11.81		7.164(1)	7.327(2)	325.67	10.19
SiO_2-LaF_3:Ho^{3+} (900°C)	$GC1_{900}$	13.99	$\alpha = \beta = 90°$ $\gamma = 120°$	7.207(1)	7.364(1)	331.22	10.33
	$GC2_{900}$	19.16		7.192(1)	7.352(2)	329.31	11.03
	$GC3_{900}$	23.09		7.204(1)	7.360(2)	330.76	10.45
	$GC4_{900}$	25.06		7.202(4)	7.356(9)	330.51	9.89
	$GC5_{900}$	22.61		7.189(1)	7.341(3)	328.59	9.35
	$GC6_{900}$	18.28		7.172(1)	7.324(1)	326.28	10.70

*R [%] – weighted profile

The performed structural characterization of prepared series of Ho^{3+}-doped sol-gel materials involved the calculations of lattice parameters and unit cell volume of crystallized LaF_3 phase. According to the lanthanides contraction phenomenon, since the ionic radius of Ho^{3+} ion ($r_{Ho(III)}$) is quite smaller than that of La^{3+} ($r_{La(III)}$) [1], we could expect that entering of Ho^{3+} ions into LaF_3 nanocrystals should result in a progressive decrease in the lattice parameters and the cell volume compared to the reference values for pure LaF_3 phase (a_0 = b_0 = 7.184 Å, c_0 = 7.351 Å; V_0 = 328.56 Å^3). Interestingly, as was presented in Table S1, the considered parameters (for both of the prepared series) are increased, except for the samples with the highest concentration of Ho^{3+} ions ($GC6_x$, with nominal La^{3+}:Ho^{3+} molar ratio set on 0.88:0.12). Indeed, for nano-glass-ceramics fabricated at 700ºC, the lattice parameters reached even a = 7.192(2) Å and c = 7.353(3) Å with unit cell volume equaled to 329.36 Å^3 ($GC3_{700}$), which were finally reduced to a = 7.164(1) Å and c = 7.327(2) Å (V = 325.67 Å^3) ($GC6_{700}$); meanwhile for samples annealed at 900ºC, the largest lattice parameters were found for $GC1_{900}$ one (a = 7.207(1) Å and c = 7.364(1) Å, V = 331.22 Å^3), but the smallest parameters – for $GC6_{900}$ sample (a = 7.172(1) Å and c = 7.324(1) Å, V = 326.28 Å^3). It is also interesting that for both of the fabricated series, GC_{700} and GC_{900}, the (111) reflex was initially shifted towards lower 2θ angles for samples with the lowest concentration of Ho^{3+} ($GC1_x$-$GC3_x$), meanwhile for samples with increased concentration of Ho^{3+} ($GC4_x$-$GC6_x$), the reverse trend was observed. All of the observed dependencies may point to entering of Ho^{3+} ions into fluoride crystal lattice, but also to the thermal expansion, since the annealing of the as-prepared xerogels was carried out at relatively high temperatures, i.e., 700 and 900ºC [2]. Hence, to attempt a deeper interpretation of the obtained results and assess the impact of such high temperatures on lattice parameters, we compared those data with our previous studies. For analogous SiO_2-LaF_3 sol-gel systems doped with Dy^{3+} ions ($r_{Dy(III)} > r_{Ho(III)}$), a gradual and well-observable decrease in the lattice parameters was denoted from a = 7.181(8) Å and c = 7.359(4) Å (for sample with La^{3+}:Dy^{3+} molar ratio equals 0.988:0.012) to a = 7.077(2) Å and c = 7.242(9) Å (for sample with high Dy^{3+} concentration; La^{3+}:Dy^{3+} molar ratio set on 0.7:0.3) [3]. Even greater modifications in lattice parameters were noted for SiO_2-LaF_3 nano-glass-ceramics co-doped with Gd^{3+}/Eu^{3+} ions ($r_{Eu(III)} > r_{Gd(III)} > r_{Ho(III)}$) [4]. For the latter series of sol-gel materials, the decrease in lattice parameters was particularly noticeable with the continuously growing Gd^{3+} concentration from a = 7.133(6) Å and c = 7.360(9) Å (for sample with La^{3+}:Gd^{3+}:Eu^{3+} =0.9:0.05:0.05 molar ratio) to a = 6.914(1) Å and c = 7.102(8) Å (for La^{3+}:Gd^{3+}:Eu^{3+} = 0.05:0.90:0.05). Thus, our previous results clearly indicate that the efficiency of RE^{3+} ions' incorporation (i.e., Dy^{3+}, Eu^{3+}, and Gd^{3+}) into the LaF_3 nanophase increased progressively with growth in their concentration, which was manifested by a substantial decrease in the crystal lattice parameters. However, it should be additionally noted that the above-mentioned sol-gel nano-glass-ceramics were obtained by controlled heat-treatment carried out at a significantly lower temperature (350ºC) compared with

the conditions applied in this work; thus, the impact of thermal expansion on crystal lattice parameters is significantly limited. Moreover, it should be clarified that in this experiment, the concentrations of the optically active ions (Ho^{3+}) are considerably lower than those of Dy^{3+}, Eu^{3+}, and Gd^{3+} in our earlier papers [3,4], which may also affect the correspondingly smaller differences in the modifications of the crystal lattice parameters.

On the other hand, the impact of the thermal expansion on crystal lattice parameters – as a consequence of heat-treatment performed at higher temperature levels, especially at 700 and 900ºC – is well-visible and described in our earlier paper concentrated on analogous SiO_2-LaF_3:Pr^{3+} nano-glass-ceramics with equivalent La^{3+}:Pr^{3+} molar ratios to La^{3+}:Ho^{3+} [5]. Due to the fact that Pr^{3+} ions are characterized by a quite comparable ionic radius as La^{3+} ($r_{Pr(III)} \approx r_{La(III)}$), it could be assumed that the impact of Pr^{3+} incorporation inside LaF_3 nanophase on the crystal lattice parameters is negligible, and – indeed – their changes were influenced mainly by the thermal expansion. Hence, we could tentatively expect that if Ho^{3+} ions (with a much smaller ionic radius than Pr^{3+}, $r_{Pr(III)} > r_{Ho(III)}$) were partially incorporated inside the fluoride nanocrystals, the parameters of the crystal lattice (and also the unit cell volumes adequately) should be decreased for series of Ho^{3+}-doped nano-glass-ceramics compared to parameters estimated for samples doped with Pr^{3+} ions. In fact, for the series of Ho^{3+}-doped sol-gel samples, the unit cell parameters are mostly reduced compared to those doped with Pr^{3+} ions, which allows us to tentatively speculate that Ho^{3+} ions were partially incorporated into the LaF_3 nanocrystals both during heat-treatment performed at 700 and 900ºC.

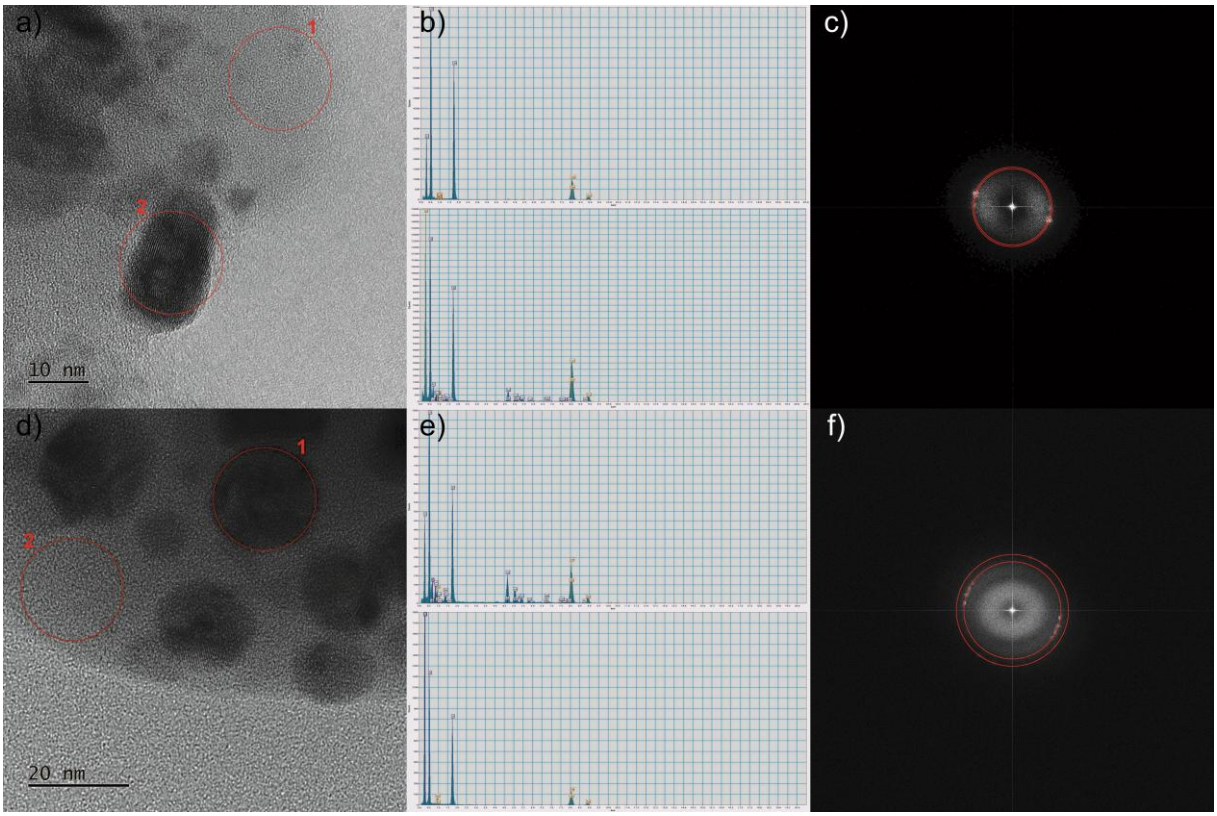

Fig. S1 TEM observations of $GC6_{700}$ (a-c) and $GC6_{900}$ (d-f) nano-glass-ceramic samples: enlargement of the edge region showing the nanocrystals and the amorphous host regions with red circles (a, d), which indicate the area used in the EDS analysis (b, e). FFT with the theoretical lattice distances marked by the red rings (c, f) were also presented.

The results from energy-dispersive X-ray spectroscopy (EDS), presented in Fig. S1(b, e) of the edge regions for $GC6_{700}$ (Fig. S1a) and $GC6_{900}$ (Fig. S1d) confirmed that the nanocrystals consist primarily of lanthanum and fluorine, with holmium admixtures. Simultaneously, EDS analysis revealed that the amorphous part of the host matrix predominantly comprises silicon oxide. The crystallization of the LaF_3 phase inside the silicate sol-gel host was also confirmed by fast Fourier transform analysis (FFT, Figs. S1(c, f)) conducted on the acquired images, and the observed interplane distances correlate well with the theoretical values for the reference material.

2. Supporting information on excitation spectra

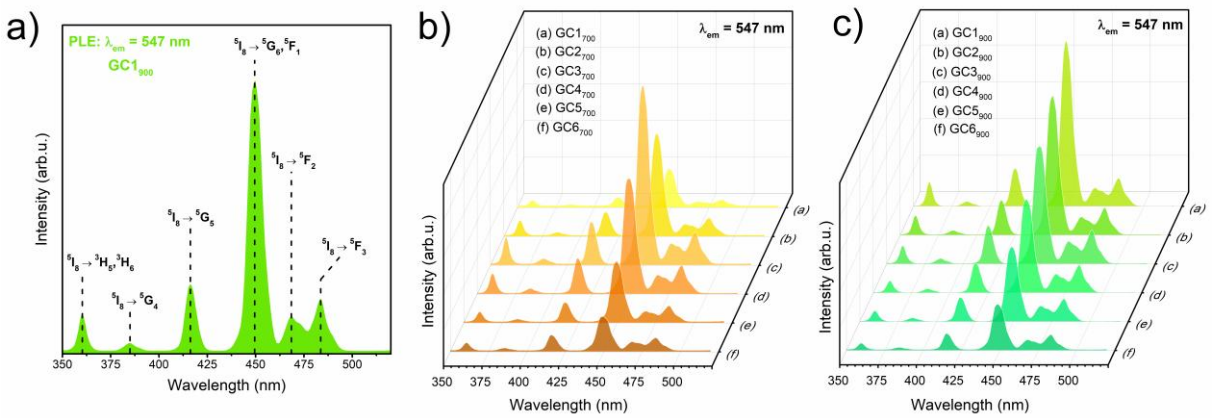

Fig. S2 The photoluminescence excitation spectra (PLE) for GCs doped with Ho^{3+} ions, recorded by monitoring λ_{em} = 547 nm luminescence: for representative $GC1_{900}$ sample with marked electronic transitions (a), presented as a function of increasing Ho^{3+} concentration in samples fabricated at 700ºC (b) and 900ºC (c).

The concentration-dependent photoluminescence excitation spectra (PLE) recorded for both series of Ho^{3+}-doped GC_{700} and GC_{900} samples were presented in Fig. S2. The spectra were registered by collecting the green luminescence of Ho^{3+} at λ_{em} = 547 nm wavelength, corresponding to the ($^5S_2$,$^5F_4$) → $^5I_8$ transition. In Fig. S2a, the exhibited PLE spectrum was recorded for representative $GC1_{900}$ sample; the observed bands correspond to the $4f^{10}$-$4f^{10}$ transitions from the $^5I_8$ ground level to the upper-lying states: ($^3H_5$,$^3H_6$) (359 nm), $^5G_4$ (384 nm), $^5G_5$ (415 nm), ($^5G_6$,$^5F_1$) (450 nm), $^5F_2$ (468 nm), and $^5F_3$ (483 nm). Figs. S2b and S2c shows the collected PLE spectra as a function of modified La^{3+}:Ho^{3+} molar ratio of samples annealed at 700 and 900ºC, respectively. For the GC_{700} series, the intensity of individual excitation bands undergoes augmentation with a gradual increase of Ho^{3+} concentration from $GC1_{700}$ (with La^{3+}:Ho^{3+} molar ratio equals to 0.997:0.003) to $GC3_{700}$ (La^{3+}:Ho^{3+} molar ratio equals to 0.988:0.012); however further increasing in Ho^{3+} content results in progressively diminishing in bands' intensities. In the case of glass-ceramics from the GC_{900} series, the well-visible decrease in excitation bands' intensities is observed from $GC1_{900}$ sample with the lowest concentration of Ho^{3+} ions (La^{3+}:Ho^{3+} molar ratio = 0.997:0.003), and it is progressively continued up to $GC6_{900}$ sample with the highest concentration of optically active Ho^{3+} ions (La^{3+}:Ho^{3+} = 0.88:0.12). The observed spectroscopic behavior evidently points to the activation of concentration quenching channels (CQ_{Ho}) in studied sol-gel materials. It is worth to mentioning that independently from heat-treatment conditions of as-prepared xerogels, the PLE excitation bands profile was kept.

3. Supporting information on emission spectra (VIS range)

Table S2. Percentage contribution (β) of individual PL bands in VIS light scope.

Series	Sample	$4f^{10}$-$4f^{10}$ transition of Ho^{3+}			
		$^5F_{2,3} \rightarrow {}^5I_8$ (β_{blue})	$(^5S_2,^5F_4) \rightarrow {}^5I_8$ (β_{green})	$^5F_5 \rightarrow {}^5I_8$ (β_{red})	$(^5S_2,^5F_4) \rightarrow {}^5I_7$ ($\beta_{red/NIR}$)
SiO_2-LaF_3:Ho^{3+} (700°C)	$GC1_{700}$	4.6%	31.9%	62.0%	1.5%
	$GC2_{700}$	4.2%	44.7%	48.8%	2.3%
	$GC3_{700}$	3.0%	61.7%	31.7%	3.6%
	$GC4_{700}$	5.0%	46.6%	45.5%	2.9%
	$GC5_{700}$	5.0%	14.0%	80.0%	1.0%
	$GC6_{700}$	5.1%	12.5%	81.6%	0.8%
SiO_2-LaF_3:Ho^{3+} (900°C)	$GC1_{900}$	0.7%	91.5%	2.6%	5.2%
	$GC2_{900}$	1.5%	90.5%	2.9%	5.1%
	$GC3_{900}$	1.4%	88.4%	4.7%	5.5%
	$GC4_{900}$	2.5%	78.6%	12.6%	6.3%
	$GC5_{900}$	4.9%	57.1%	33.1%	4.9%
	$GC6_{900}$	4.5%	40.1%	52.9%	2.5%

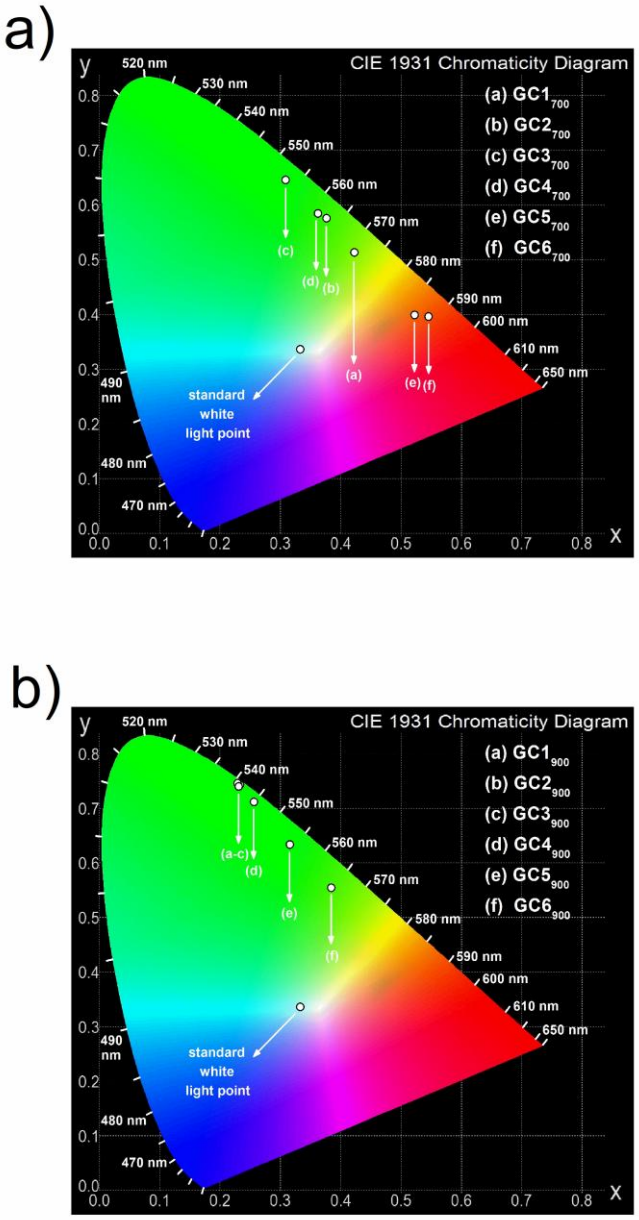

Fig. S3 CIE chromaticity diagrams for samples fabricated at 700ºC (a) and 900ºC (b).

Table S3. CIE chromaticity coordinates calculated for prepared Ho^{3+}-doped sol-gel nano-glass-ceramics, compared with the data from the literature.

Series	Sample	Excitation wavelength	CIE (x‖y)	Color of emitted light	Ref.
SiO_2-LaF_3:Ho^{3+} (700°C)	$GC1_{700}$	λ_{ex} = 450 nm	(0.422‖0.510)	yellow	[this work]
	$GC2_{700}$		(0.376‖0.572)	green	
	$GC3_{700}$		(0.309‖0.642)	green	
	$GC4_{700}$		(0.362‖0.581)	green	
	$GC5_{700}$		(0.521‖0.396)	orange	
	$GC6_{700}$		(0.544‖0.393)	orange	
SiO_2-LaF_3:Ho^{3+} (900°C)	$GC1_{900}$	λ_{ex} = 450 nm	(0.234‖0.739)	green	[this work]
	$GC2_{900}$		(0.230‖0.742)	green	
	$GC3_{900}$		(0.232‖0.736)	green	
	$GC4_{900}$		(0.257‖0.708)	green	
	$GC5_{900}$		(0.316‖0.630)	green	
	$GC6_{900}$		(0.384‖0.551)	green	
zinc fluorophosphate (ZFP) glasses	0.1 mol% Ho^{3+}	λ_{ex} = 450 nm	(0.39‖0.57)	yellow	[6]
	0.3 mol% Ho^{3+}		(0.38‖0.57)		
	0.5 mol% Ho^{3+}		(0.32‖0.58)		
	1.0 mol% Ho^{3+}		(0.29‖0.58)	green	
	1.5 mol% Ho^{3+}		(0.34‖0.58)	yellow	
lead tungsten tellurite glasses	0.1 mol% Ho^{3+}	λ_{ex} = 452 nm	(0.3082‖0.6819)	green	[7]
	0.5 mol% Ho^{3+}		(0.2879‖0.7031)		
	1.0 mol% Ho^{3+}		(0.2858‖0.7069)		
	1.5 mol% Ho^{3+}		(0.2844‖0.7070)		
	2.0 mol% Ho^{3+}		(0.2780‖0.7126)		
	2.5 mol% Ho^{3+}		(0.3022‖0.6911)		
zinc alumino bismuth borate glasses	0.1 mol% Ho^{3+}	λ_{ex} = 586 nm	(0.59‖0.35)	red	[8]
	0.5 mol% Ho^{3+}		(0.60‖0.34)		
	1.0 mol% Ho^{3+}		(0.62‖0.33)		
	1.5 mol% Ho^{3+}		(0.60‖0.30)		
	2.0 mol% Ho^{3+}		(0.60‖0.29)		
	2.5 mol% Ho^{3+}		(0.59‖0.28)		
boro phosphate glass-ceramics (0.5 mol%)	without addition of Ag NPs	λ_{ex} = 450 nm	(0.350‖0.640)	green	[9]
	0.6 mol% Ag NPs		(0.350‖0.630)		
	0.8 mol% Ag NPs		(0.360‖0.630)		

As was presented in Fig. S3 and Table S3, for samples heat-treated at 700ºC with the lowest concentration of Ho^{3+} ions, i.e., $GC1_{700}$-$GC3_{700}$, the coordinates are lying between (0.422|0.510) and (0.309|0.642) points; thus, the resultant colors of the obtained emissions shift from yellow-toned light region ($GC1_{700}$ with dominant wavelength λ_d = 570 nm) to green ($GC2_{700}$ with λ_d = 561 nm, $GC3_{700}$ with λ_d = 550 nm). For the last samples from the series with the highest concentration of Ho^{3+} ions ($GC4_{700}$-$GC6_{700}$), the coordinates shift from (0.362|0.581) to (0.544|0.393). Resultantly, the color of emitted light modifies from green ($GC4_{700}$ with λ_d = 558 nm) to orange ($GC5_{700}$ with λ_d = 590 nm, $GC6_{700}$ with λ_d = 593 nm). In the case of a series fabricated by heat-treatment carried out at 900ºC, all samples emit green light described by coordinates ranging from (0.234|0.739) to (0.384|0.551). It should be noted that the tonality of emitted green luminescence was continuously changed with increasing Ho^{3+} concentration, and the dominant wavelength modified from λ_d = 540 nm ($GC1_{900}$-$GC3_{900}$), through λ_d = 544 nm ($GC4_{900}$), λ_d = 551 nm ($GC5_{900}$), up to λ_d = 563 nm ($GC6_{900}$). Such observed shifting in green light tonality corresponds to the increasing involvement of the red luminescence component assigned to the $^5F_5 \rightarrow {}^5I_8$ transition. Moreover, it should also be emphasized that the generated green light by fabricated Ho^{3+}-doped sol-gel glass-ceramics – especially for $GC3_{700}$ and $GC5_{900}$ samples – is lying nearby the standard point of the green illuminant (0.290|0.600) governed by the European Broadcasting Union (EBU) [10]. The similar CIE chromaticity coordinates – as for prepared sol-gel green emitters – were found in the literature for Ho^{3+}-doped boro-phosphate glass-ceramics and Ho^{3+}-doped lead tungsten tellurite glasses [7, 9]. To further characterize the quality of the generated emission, McCamy's formula was used for calculations of correlated color temperature (CCT) [11]:

$$CCT = -449n^3 + 3525n^2 - 6823n + 5520.33, \quad (1)$$

in which $n = (x - x_e)/(y - y_e)$ (x_e = 0.332, y_e = 0.186; the epicenter of the isotemperature lines). The color purity (CP) was additionally calculated based on the below formula [12]:

$$CP = \frac{\sqrt{(x - x_i)^2 + (y - y_i)^2}}{\sqrt{(x_d - x_i)^2 + (y_d - y_i)^2}} \cdot 100\%, \quad (2)$$

in which (x, y) are the chromaticity coordinates, (x_i, y_i) are the coordinates of standard white light (0.333|0.333), and (x_d, y_d) are the chromaticity coordinates of the dominant wavelength (λ_d). For the GC_{700} series, the CCT values for the subsequent samples were estimated at: 3887, 4788, 5874, 5022, 1907, and 1747 K; meanwhile, for the GC_{900} series, the values of CCT parameter equal to: 6845, 6894, 6880, 6575, 6575, 5771, as well as 4618 K. Thus, it could be observed that growing involvement of the $^5F_5 \rightarrow {}^5I_8$ red luminescence (expressed as β_{red}

coefficient) in recorded PL spectra (Fig. 3 in manuscript), contributes to the tunability of generated emission from cool-toned to warm-toned shades. Moreover, the CP values were estimated at 80.7%, 85.9%, and 88.0% for resultant green luminescence emitted by $GC1_{700}$-$GC3_{700}$ samples; the CP for yellow light (emitted by $GC4_{700}$ sample) was assessed on 84.4%, while the CP values for orange luminescence (produced by $GC5_{700}$ and $GC6_{700}$ glass-ceramics) were established on 76.4% and 82.4%, respectively. In the case of green photoluminescence generated by all samples from the GC_{900} series, the CP values range from 81.6% ($GC6_{900}$) even to 98.0% ($GC2_{900}$). Thus, the collected experimental results clearly proved that the quality of emitted light is satisfactory.

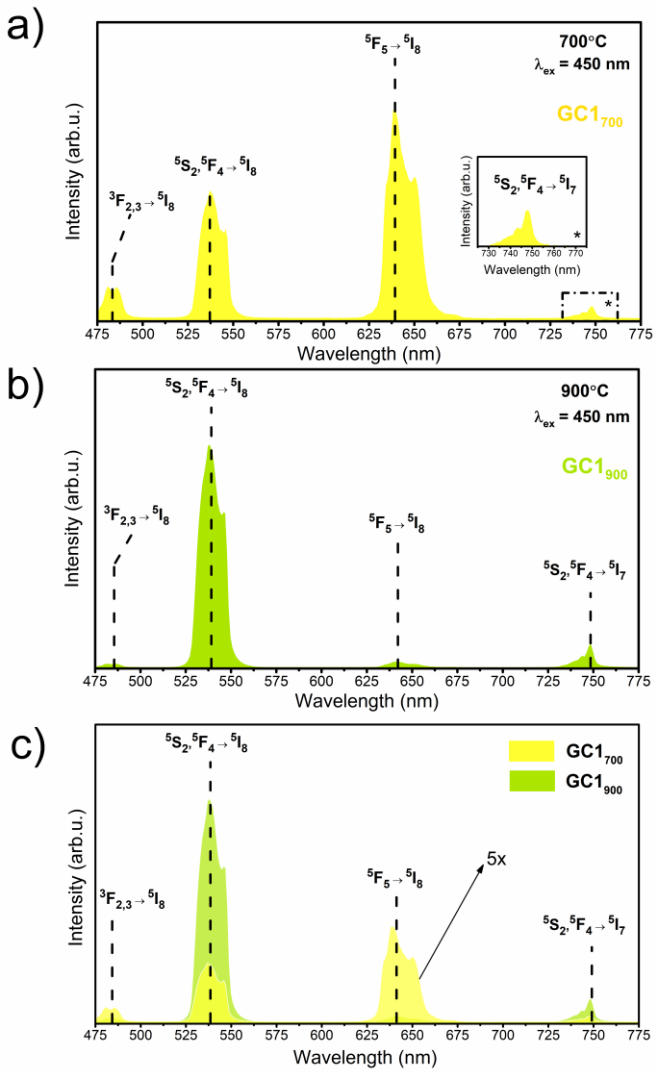

Fig. S4 The impact of elevated temperature on PL spectra in VIS range for representative $GC1_{700}$ (a) and $GC1_{900}$ (b) samples with equivalent nominal concentration of Ho^{3+} ions, as well as the comparison of their luminescence intensities (c).

4. Supporting information on emission spectra (NIR region)

Table S4. Percentage contribution (β) of individual PL bands in NIR spectral region.

Series	Sample	$4f^{10}$-$4f^{10}$ transition of Ho^{3+}				
		$^5F_5 \rightarrow {}^5I_7$ ($\beta_{NIR/0.97\mu m}$)	$(^5S_2,^5F_4) \rightarrow {}^5I_6$ ($\beta_{NIR/1.02\mu m}$)	$^5I_6 \rightarrow {}^5I_8$ ($\beta_{NIR/1.19\mu m}$)	$(^5S_2,^5F_4) \rightarrow {}^5I_5$ ($\beta_{NIR/1.35\mu m}$)	$^5F_5 \rightarrow {}^5I_6$ ($\beta_{NIR/1.45\mu m}$)
SiO_2-LaF_3:Ho^{3+} (700°C)	$GC1_{700}$	16.0%	6.5%	9.5%	24.3%	43.7%
	$GC2_{700}$	9.5%	8.5%	14.1%	25.4%	42.5%
	$GC3_{700}$	5.0%	11.8%	29.8%	29.5%	23.9%
	$GC4_{700}$	7.7%	6.8%	40.5%	18.5%	26.5%
	$GC5_{700}$	23.7%	1.5%	11.7%	11.4%	51.7%
	$GC6_{700}$	20.3%	-	12.8%	3.8%	63.1%
SiO_2-LaF_3:Ho^{3+} (900°C)	$GC1_{900}$	-	6.3%	79.1%	14.6%	-
	$GC2_{900}$	-	3.8%	87.0%	9.0%	0.2%
	$GC3_{900}$	-	7.4%	72.4%	19.3%	0.9%
	$GC4_{900}$	0.5%	0.1%	86.3%	11.0%	2.1%
	$GC5_{900}$	0.4%	0.5%	95.3%	1.7%	2.1%
	$GC6_{900}$	0.1%	0.3%	97.3%	1.1%	1.2%

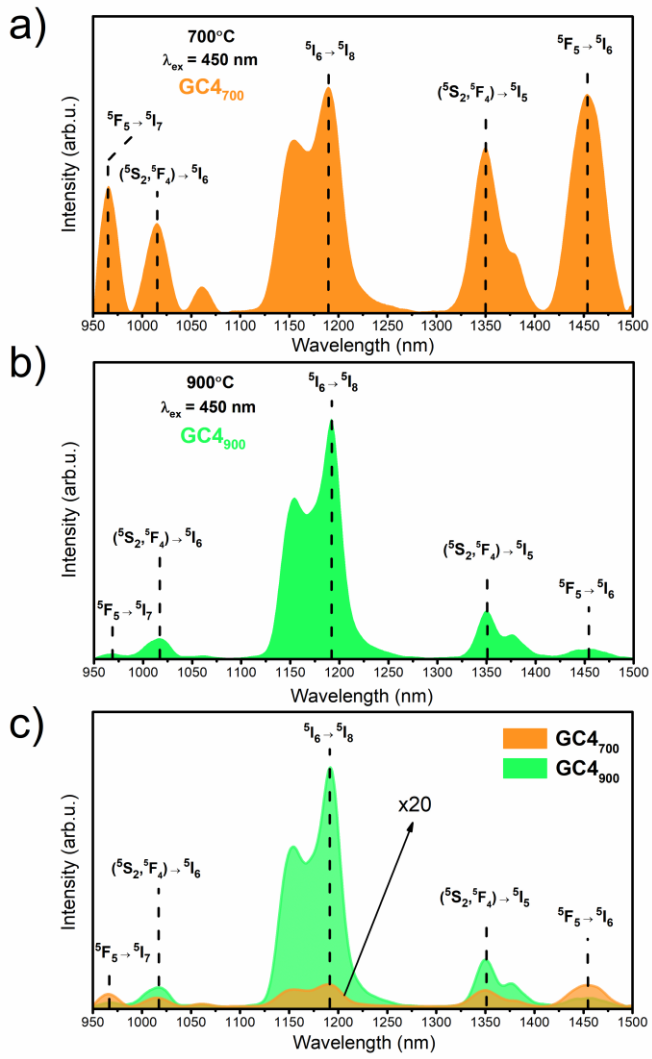

Fig. S5 The impact of elevated temperature on PL spectra in NIR range for representative $GC4_{700}$ (a) and $GC4_{900}$ (b) GCs with the same nominal concentration of Ho^{3+} ions, as well as the comparison of their luminescence intensities (c).

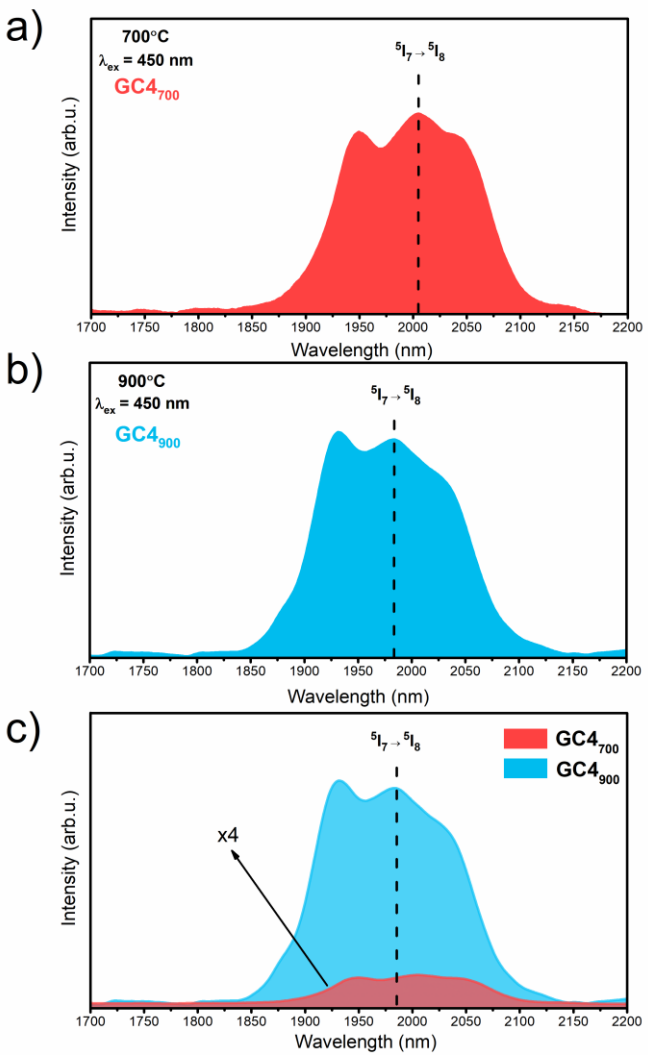

Fig. S6 The impact of elevated temperature on PL spectra in MIR scope for representative $GC4_{700}$ (a) and $GC4_{900}$ (b) samples with equivalent nominal concentration of Ho^{3+} ions, as well as the comparison of their luminescence intensities (c).

5. Supporting information on decay analysis

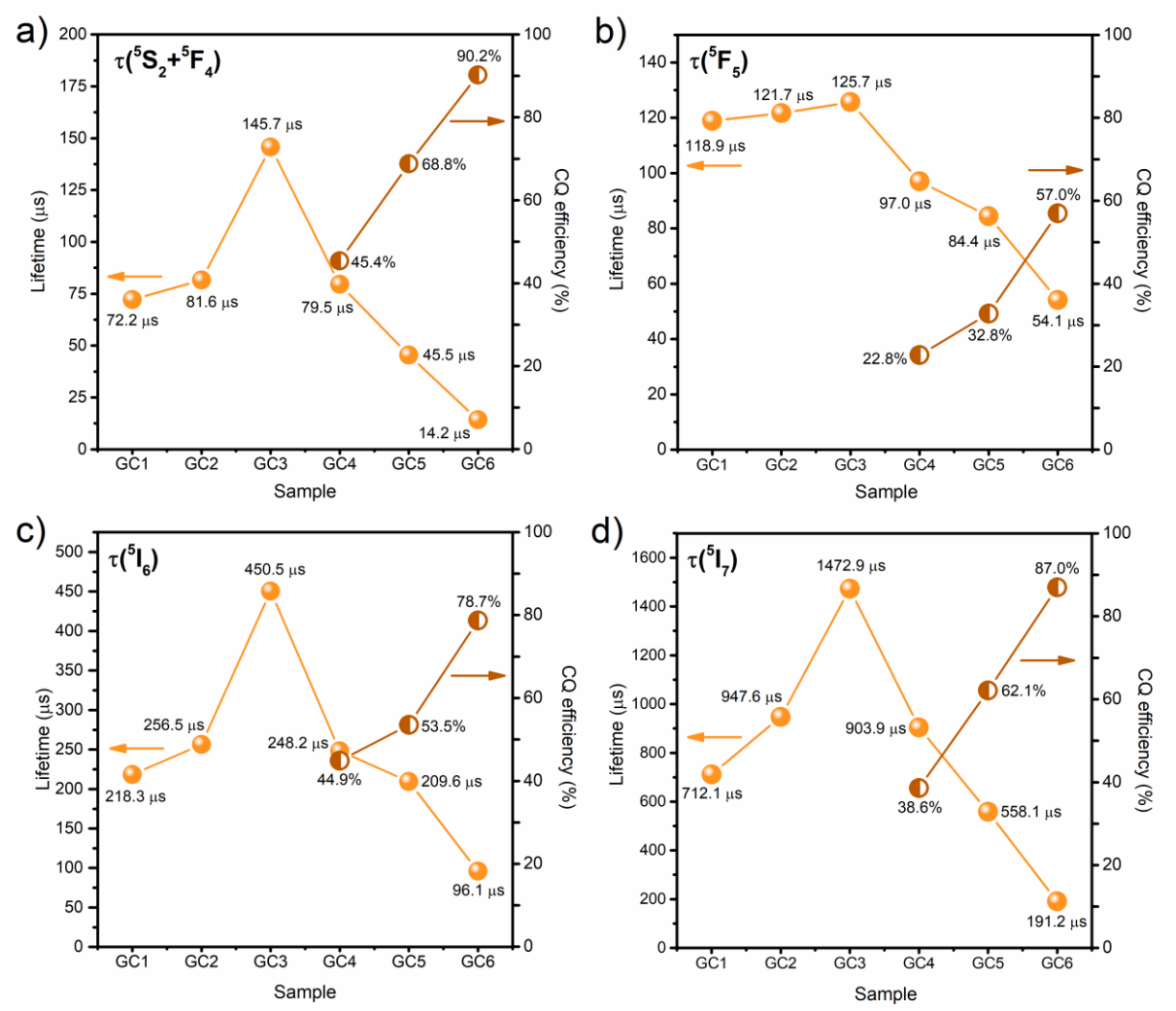

Fig. S7 Correlations in luminescence decay times and concentration quenching efficiencies for GC_{700} samples with increasing Ho^{3+} concentration.

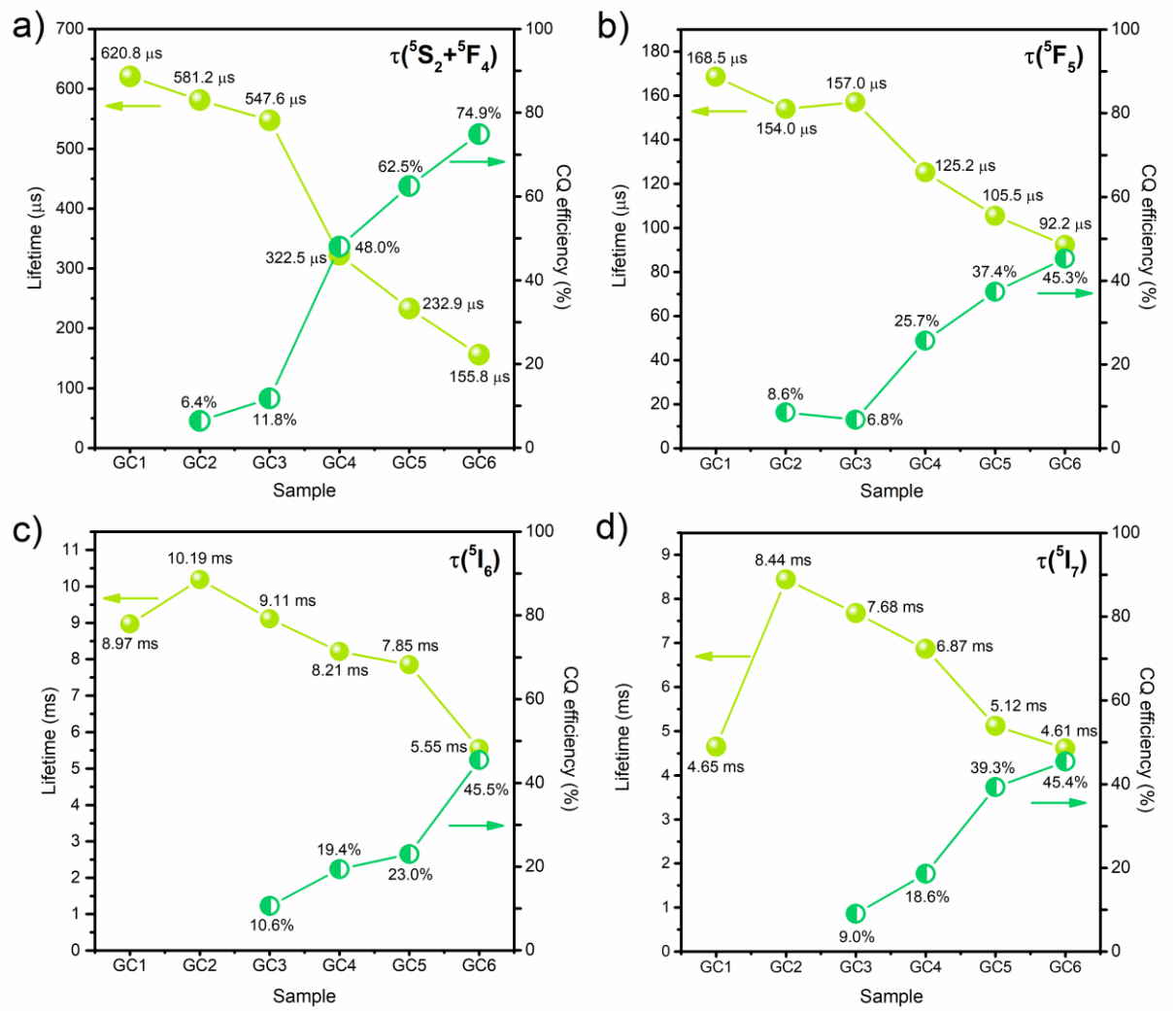

Fig. S8 Correlations in luminescence decay times and concentration quenching efficiencies for GC_{900} samples with increasing Ho^{3+} concentration.

The calculated efficiencies of CQ_{Ho} processes for all analyzed excited levels, i.e., ($^5S_2$,$^5F_4$), $^5F_5$, $^5I_6$, and $^5I_7$, progress faster for samples obtained by annealing performed at 700ºC. Factually, the PL spectra and assessed percentage contribution of the individual emission bands could suggest that the incorporation of Ho^{3+} ions into the LaF_3 crystalline phase is more efficient for samples from the GC_{900} series, than for glass-ceramics from the GC_{700} series. On the other hand, based on the average sizes of precipitated LaF_3 crystals inside the amorphous silicate sol-gel network and relative amounts of crystal fraction (which could be assumed from intensities of individual XRD reflexes), it is reasonable to expect that the average Ho^{3+}-Ho^{3+} inter-ionic distances inside fluoride crystal lattice seem to be somewhat elongated for glass-ceramics annealed at 900ºC (compared to analogous samples from the GC_{700} series with equivalent nominal concentration), even though their segregation inside fluoride crystal phase is higher. This hypothesis could explain why the concentration quenching process of Ho^{3+} ions (CQ_{Ho}) is less efficient for materials heat-treated at a higher temperature, i.e., 900ºC.

Table S5. Luminescence decay times for individual excited states of Ho^{3+} ions in prepared GCs compared with the data from literature.

a) lifetimes for the ($^5S_2$,$^5F_4$) excited level

Excited state	Type of material	Sample	Decay time	Ref.
($^5S_2$,$^5F_4$)	SiO_2-LaF_3:Ho^{3+} GCs (700°C)	$GC1_{700}$	72.2 µs	[this work]
		$GC2_{700}$	81.6 µs	
		$GC3_{700}$	145.7 µs	
		$GC4_{700}$	79.5 µs	
		$GC5_{700}$	45.5 µs	
		$GC6_{700}$	14.2 µs	
	SiO_2-LaF_3:Ho^{3+} GCs (900°C)	$GC1_{900}$	620.8 µs	[this work]
		$GC2_{900}$	581.2 µs	
		$GC3_{900}$	547.6 µs	
		$GC4_{900}$	322.5 µs	
		$GC5_{900}$	232.9 µs	
		$GC6_{900}$	155.8 µs	
	$Y_2Zr_2O_7$:Ho^{3+} transparent ceramics	1 mol% Ho^{3+}	42 µs	[13]
		2 mol% Ho^{3+}	48 µs	
		3 mol% Ho^{3+}	40 µs	
		4 mol% Ho^{3+}	36 µs	
	Ho^{3+}-doped germanate glasses	0.1% Ho^{3+}	21 µs	[14]
		0.5% Ho^{3+}	18 µs	
		1.0% Ho^{3+}	16 µs	
		1.5% Ho^{3+}	25 µs	
		2.5% Ho^{3+}	16 µs	
	Ho^{3+}/Yb^{3+} co-doped silica glass and glass-ceramics	glass	1 µs	[15]
		GC (650°C)	1 µs	
		GC (675°C)	7 µs	
		GC (700°C)	10 µs	
		GC (725°C)	11 µs	

b) lifetimes for the $^5F_5$ excited level

Excited state	Type of material	Sample	Decay time	Ref.
$^5F_5$	SiO_2-LaF_3:Ho^{3+} GCs (700°C)	$GC1_{700}$	118.9 µs	[this work]
		$GC2_{700}$	121.7 µs	
		$GC3_{700}$	125.7 µs	
		$GC4_{700}$	97.0 µs	
		$GC5_{700}$	84.4 µs	
		$GC6_{700}$	54.1 µs	
	SiO_2-LaF_3:Ho^{3+} GCs (900°C)	$GC1_{900}$	168.5 µs	[this work]
		$GC2_{900}$	154.0 µs	
		$GC3_{900}$	157.0 µs	
		$GC4_{900}$	125.2 µs	
		$GC5_{900}$	105.5 µs	
		$GC6_{900}$	92.2 µs	
	Ho^{3+}-doped transparent ceramics	Y_2O_3:Ho^{3+}	103.7 µs	[16]
		$Y_3Al_5O_{12}$:Ho^{3+}	3.47 µs	

c) lifetimes for the $^5I_6$ excited level

Excited state	Type of material	Sample	Decay time	Ref.
$^5I_6$	SiO_2-LaF_3:Ho^{3+} GCs (700°C)	$GC1_{700}$	218.3 µs	[this work]
		$GC2_{700}$	256.5 µs	
		$GC3_{700}$	450.5 µs	
		$GC4_{700}$	248.2 µs	
		$GC5_{700}$	209.6 µs	
		$GC6_{700}$	96.1 µs	
	SiO_2-LaF_3:Ho^{3+} GCs (900°C)	$GC1_{900}$	8.97 ms	[this work]
		$GC2_{900}$	10.19 ms	
		$GC3_{900}$	9.11 ms	
		$GC4_{900}$	8.21 ms	
		$GC5_{900}$	7.85 ms	
		$GC6_{900}$	5.55 ms	
	Ho^{3+}-doped transparent ceramics	Y_2O_3:Ho^{3+}	928 µs	[16]
		$Y_3Al_5O_{12}$:Ho^{3+}	44.9 µs	

d) lifetimes for the $^5I_7$ excited level

Excited state	Type of material	Sample	Decay time	Ref.
$^5I_7$	SiO_2-LaF_3:Ho^{3+} GCs (700°C)	$GC1_{700}$	712.1 µs	[this work]
		$GC2_{700}$	947.6 µs	
		$GC3_{700}$	1472.9 µs	
		$GC4_{700}$	903.9 µs	
		$GC5_{700}$	558.1 µs	
		$GC6_{700}$	191.2 µs	
	SiO_2-LaF_3:Ho^{3+} GCs (900°C)	$GC1_{900}$	4.65 ms	[this work]
		$GC2_{900}$	8.44 ms	
		$GC3_{900}$	7.68 ms	
		$GC4_{900}$	6.87 ms	
		$GC5_{900}$	5.12 ms	
		$GC6_{900}$	4.61 ms	
	Ho^{3+}-doped transparent ceramics	Y_2O_3:Ho^{3+}	10.92 ms	[16]
		$Y_3Al_5O_{12}$:Ho^{3+}	7.04 ms	
	$(Lu,Sc)_2O_3$:Ho^{3+} transparent ceramics	1.4 at% Ho	9.0 ms	[17]
		3 at% Ho	5.5 ms	
	sol-gel silica glasses with modified Al:Si ratio (0.2% mol Ho^{3+})	Al:Si = 1.0:98.8	0.91 ms	[18]
		Al:Si = 2.0:97.8	1.04 ms	
		Al:Si = 3.0:96.8	1.19 ms	
		Al:Si = 4.0:95.8	1.23 ms	
		Al:Si = 5.0:94.8	1.33 ms	
	CaF_2:Ho^{3+} transparent ceramics	0.5% mol Ho^{3+}	30.7 ms	[19]
		1% mol Ho^{3+}	29.1 ms	
		2% mol Ho^{3+}	27.9 ms	
		3% mol Ho^{3+}	25.4 ms	
		5% mol Ho^{3+}	25.3 ms	
	Y_3NbO_7:Ho^{3+} transparent ceramic	0.6% mol Ho^{3+}	8.09 ms	[20]

6. References

[1] P. D'Angelo, A. Zitolo, V. Migliorati, G. Chillemi, M. Duvail, P. Vitorge, S. Abadie, and R. Spezia, *Inorg. Chem.*, 2011, **50**, 4572-4579.

[2] W. Korczak and P. Mikołajczak, *J. Cryst. Growth*, 1983, **61**, 601-605.

[3] N. Pawlik, T. Goryczka, E. Pietrasik, J. Śmiarowska, and W.A. Pisarski, *Nanomater.*, 2022, **12**, 4500.

[4] N. Pawlik, B. Szpikowska-Sroka, T. Goryczka, and W.A. Pisarski, *Ceram. Int.*, 2023, **49**, 41041-41053.

[5] N. Pawlik, T. Goryczka, M. Zubko, J. Śmiarowska, and W.A. Pisarski, *Nanoscale*, 2024, **16**, 4249-4265.

[6] V. Reddy Prasad, S. Damodaraian, and Y.C. Ratnakaram, *Opt. Mater.*, 2018, **78**, 63-71.

[7] M. Venkateswarlu, Sk. Mahamuda, K. Swapna, M.V.V.K.S. Prasad, A. Srinivasa Rao, S. Shakya, A. Mohan Babu, and G. Vijaya Prakash, *J. Lumin.*, 2015, **163**, 54-71.

[8] Sk. Mahamuda, K. Swapna, P. Packiyaraj, A. Srinivasa Rao, and G. Vijaya Prakash, *Opt. Mater.*, 2013, **36**, 362-371.

[9] A.S. Alqarni, R. Hussin, S.N. Alamri, and S.K. Ghoshal, *J. Lumin.*, 2020, **223**, 117218.

[10] C.K. Kesavulu, H.J. Kim, S.W. Lee, J. Kaewkhao, E. Kaewnuam, and N. Wantana, *J. Alloy. Compd.*, 2017, **704**, 557-564.

[11] V. Singh, A.A. Bhat, A.R. Kadam, S. Saravanakumar, P. K. Tripathi, S.J. Dhoble, and J.B. Joo, *J. Electron. Mater.*, 2024, **53**, 6384-6394.

[12] Y.-F. Wu, Y.-T. Nien, Y.-J. Wang, and I.-G. Chen, *J. Am. Ceram. Soc.*, 2012, **95**, 1360-1366.

[13] Y. Ye, Z. Tang, Z. Ji, H. Xiao, Y. Liu, Y. Qin, L. Liang, J. Qi, and T. Lu, *Opt. Mater.*, 2021, **121**, 111643.

[14] M. Ravi Prakash, G. Neelima, V.K. Kummara, N. Ravi, C.S. Dwaraka Viswanath, T. Subba Rao, and S. Mahaboob Jilani, *Opt. Mater.*, 2019, **94**, 436-443.

[15] P. Babu, U.R. Rodríguez-Mendoza, V. Lavín, and R. Praveena, *Opt. Mater.*, 2024, **153**, 115609.

[16] P. Loiko, L. Basyrova, R. Maksimov, V. Shitor, M. Baranov, F. Starecki, X. Mateos, and P. Camy, *J. Lumin.*, 2021, **240**, 118460.

[17] W. Jing, P. Loiko, J.M. Serres, Y. Wang, E. Kifle, E. Vilejshikova, M. Augiló, F. Díaz, U. Griebner, H. Huang, V. Petrov, and X. Mateos, *J. Lumin.*, 2018, **203**, 145-151.

[18] X. Wang, W. Xu, S. Wang, C. Yu, D. Chen, and L. Hu, *J. Alloy. Compd.*, 2016, **657**, 478-482.

[19] Z. Wan, W. Li, B. Mei, Z. Liu, and Y. Yang, *J. Lumin.*, 2020, **223**, 117188.

[20] L. Cornet, S. Guene-Girard, J.-M. Heintz, R. Boulesteix, A. Maître, and V. Jubera, *Opt. Mater.*, 2023, **144**, 114319.